Construction and Building Materials 326 (2022) 126900

Contents lists available at ScienceDirect

Construction and Building Materials

journal homepage: www.elsevier.com/locate/conbuildmat

Uniaxial behavior of pre-stressed iron-based shape memory alloy rebars under cyclic loading reversals

Saim Raza [a], Julien Michels [b], Moslem Shahverdi [a,*]

[a] Empa, Swiss Federal Laboratories for Materials Science and Technology, Dübendorf 8600, Switzerland
[b] Re-fer AG, Seewen, Switzerland

ARTICLE INFO

Keywords:
Fe-SMA
Cyclic loading reversals
Pre-stress loss
Inelastic buckling

ABSTRACT

Iron-based shape memory alloys (Fe-SMA) have recently emerged as a promising alternative for structural design and retrofitting due to their unique self-prestressing ability. The feasibility of using Fe-SMA rebars, strips, and stirrups for improving the flexural and shear behavior of reinforced concrete beams and slabs has been successfully demonstrated in many experimental investigations. However, existing studies have mostly focused on applications where structural elements are subjected to monotonic loading. On the other hand, tension-compression reversals are mostly experienced by the reinforcement under seismic actions, which makes it necessary to characterize the pre-stress behavior of Fe-SMA under cyclic loading reversals. More specifically, it is important to identify the limit associated with the complete loss of pre-stress of Fe-SMA under tension-compression reversals. Another important research gap is the lack of understanding of the inelastic buckling behavior of Fe-SMA rebars, which is also important for the application of Fe-SMAs in seismic design and retrofitting. Specifically, an understanding of the inelastic buckling behavior is needed for determining the spiral spacing and accurate moment-curvature analysis of cross-sections of concrete columns reinforced with Fe-SMA rebars. This study aims to address these important research gaps by experimentally evaluating the stress-strain behavior of pre-stressed Fe-SMA rebars under cyclic tension-compression reversals. The outcome of this study will facilitate in developing accurate analytical and numerical models for estimating the cyclic response of Fe-SMA rebars and will also assist in developing design guidelines for the use of Fe-SMA in seismic applications.

1. Introduction

New construction technologies and retrofitting methods are employing smart materials instead of traditional materials (concrete, steel) for enhancing the capacity of the structures. Smart materials are those materials that can respond to any changes in their condition by external stimuli (stress, temperature etc.) in a controlled manner. Shape memory alloys (SMAs) belong to the family of such smart materials that offer unique characteristics such as superelasticity and shape memory effect. Superelasticity is the property due to which an SMA can recover its original undeformed shape upon unloading from large deformations. Similarly, the shape memory effect refers to the property due to which an SMA can recover inelastic deformations upon heating. Nitinol and copper-based SMAs exhibit excellent superelastic behavior, whereas iron-based shape memory alloys (Fe-SMAs) show a stable shape memory effect [1–3].

The shape memory effect of the Fe-SMAs can result in recovery stress if external constraints (e.g. clamps, anchorages etc.) are used to prevent the development of recovery strain upon heating of SMA. This recovery stress can then be used to pre-stress reinforced concrete elements to improve their serviceability and ultimate limit state behavior [4]. Pre-stressed Fe-SMA rebars and strips have been extensively used in many retrofitting applications as near-surface mounted, embedded and externally anchored reinforcement for flexural and shear strengthening of RC beams [5–17], slabs [18], and masonry walls [19]. Few recent studies have investigated the bond-slip characteristics of near-surface mounted Fe-SMA rebars [20–22] and their elevated temperature behavior for strengthening civil structures [23]. However, all the existing applications of Fe-SMA involved situations where Fe-SMA was subjected to monotonic loading. On the other hand, the unique self-prestressing ability of Fe-SMA also makes it an attractive alternative for seismic design and retrofitting applications where cyclic loading excursions are expected. The potential applications include active confinement of RC columns and walls with embedded or externally

* Corresponding author.
E-mail address: moslem.shahverdi@empa.ch (M. Shahverdi).

https://doi.org/10.1016/j.conbuildmat.2022.126900
Received 11 November 2021; Received in revised form 20 January 2022; Accepted 16 February 2022
Available online 24 February 2022

anchored pre-stressed spirals or ties. Similarly, bonded or unbonded pre-stressed Fe-SMA longitudinal reinforcement in RC columns and walls can incorporate a recentering behavior wherein the pre-stress of Fe-SMA can provide a restoring force to the structural element to return to its original position (i.e. self-centering) after strong ground motion excitations.

The recovery stress behavior of pre-stressed Fe-SMA under tension-compression reversals needs to be fully understood for using it effectively for seismic design and retrofitting applications. The material behavior of pre-stressed Fe-SMA under monotonic tensile loading has already been characterized extensively in past studies. Michels et al. [24] and Shahverdi et al. [25] studied the tensile behavior of pre-stressed Fe-SMA rebars and strips, respectively. The cyclic behavior including the energy dissipation of non-prestressed Fe-SMA rebars under large tension-compression strain reversals was recently studied in Rosa et al. [26]. However, no study has so far investigated the cyclic behavior of pre-stressed Fe-SMA under tension-compression reversals. This aspect needs attention because studies on high-cyclic tensile fatigue behavior [27,28] of pre-stressed Fe-SMA have shown partial loss of recovery stress under small amplitude tensile strain reversals. Therefore, it is particularly important to identify the strain limit associated with the total loss of recovery stress after which pre-stressed and non-prestressed Fe-SMA would start behaving identically.

The other important aspect that needs to be studied for seismic design and retrofitting applications is the buckling behavior of Fe-SMA because, under seismic loading, the pre-stressed Fe-SMA rebars would be subjected to compression reversals that might initiate buckling and the associated softening in the compressive response, which can adversely impact the load carrying and energy absorption capacity of the reinforcement. In addition, this behavior needs to be investigated for accurate moment-curvature analysis of the Fe-SMA reinforced cross-sections so that the strength and ductility are not overestimated because of neglecting the softening in response due to buckling [29]. Furthermore, for designing RC columns with Fe-SMA, this would also help to determine if the spiral or tie spacing requirements for mild steel are applicable for Fe-SMA rebars. Previous studies on reinforcing steel under reversed cyclic loading have shown that softening in the compressive regime due to the inelastic buckling occurs when the lateral support spacing (spiral spacing) is greater than five to six times the longitudinal rebar diameter [30,31]. Therefore, it is recommended that tie or spiral spacing greater than six times rebar diameter should only be used in situations where no ductility is required from the structural member [29]. It has also been reported for steel rebars that the buckling commences after a reversal from the tension cycle and strongly depends on the maximum value of tensile strain reached before the reversal [32].

With the outlined state of research and practice on Fe-SMA, the primary aim of this study is to address the two identified research gaps i.e. pre-stress behavior and inelastic buckling of Fe-SMA rebars under

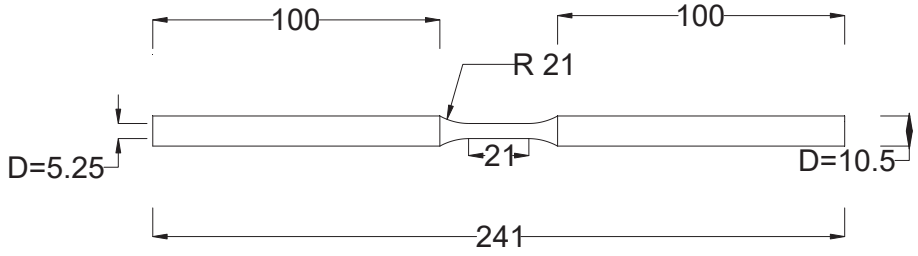

(a)

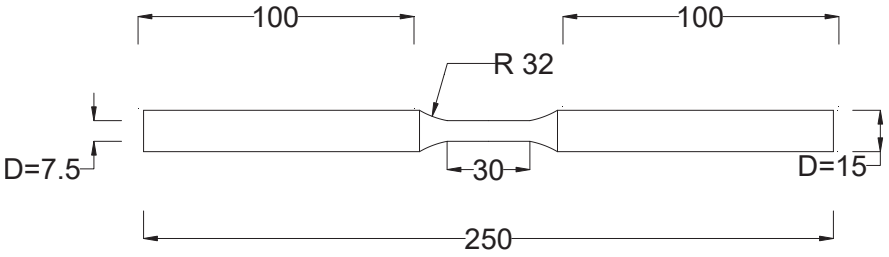

(b)

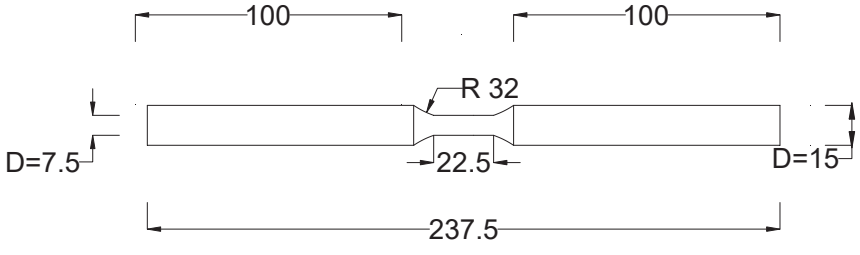

(c)

Fig. 1. Details of the dogbone specimens: a) D = 5.25 and L/D = 4; b) D = 7.5 mm and L/D = 4; c) D = 7.5 mm and L/D = 3.

tension-compression loading reversals. The following section outlines the details of the experimental testing campaign, which is followed by the results and discussion section. Finally, the work is concluded with a set of possible guidelines for using Fe-SMA with L/D = 3 and 4 for applications involving cyclic loading. The composition of Fe-SMA used in this study is Fe–17Mn–5Si–10Cr–4Ni–1(V,C) (mass%).

2. Experiments

2.1. Specimen details

The experimental campaign comprised 14 cylindrical dogbone specimens and two ribbed rebar specimens. The geometric details of the specimens are summarized in Fig. 1 and Table 1, respectively. The dogbones with 5.25 mm diameter (at the reduced section) were manufactured from ribbed Fe-SMA rebars of 10.5 mm diameter, whereas the dogbones with 7.5 mm diameter (at the reduced section) were manufactured from 16.5 mm diameter ribbed Fe-SMA rebars. The different diameters (5.25 mm and 7.5 mm) of dogbones are intended to reflect the different rebar diameters (10.5 mm and 16.5 mm) from which they are manufactured. The dogbones were designed according to the recommendations of ASTM E606/E606M-19 – Standard Test Method for Strain-Controlled Fatigue Testing [39]. The ratio of unsupported length to the diameter of the reduced section (i.e. L/D) was 4 for most of the specimens. A couple of specimens with L/D = 3 were also used to study the effect of buckling under compressive loading. In addition to the dogbone specimens, the test matrix included 10.5 mm diameter ribbed rebar specimens to identify any possible difference in the pre-stress behavior of the dogbones and the actual rebars from which the dogbones were manufactured. All the tested specimens were from the same batch.

The following three types of specimens were mainly used in the experimental campaign: non-prestrained, prestrained non-activated, and prestrained-activated. The non-prestrained specimens represent the as-received condition of the specimens from the supplier. The prestrained non-activated specimens were prepared by subjecting the as-received samples to an initial prestrain of 4% and then unloading to zero load. In contrast, the preparation of the prestrained activated specimens involved both initial prestraining as well as thermal activation for generating the initial recovery stress, as schematically shown in Fig. 2. For this purpose, an initial prestrain of 4% was first applied to the as-received samples, followed by unloading to zero load. Subsequently, the thermal activation was performed on the resulting prestrained samples to trigger the shape memory effect of Fe-SMA for generating the pre-stress/recovery stress. The procedure for thermal activation was as follows: firstly, an initial preload of 50 MPa was applied to the specimen before heating. This was done to avoid compression during the initial stages of heating when Fe-SMA undergoes thermal expansion [25]. Then, while holding the strain constant (extensometer controlled), the specimen was heated from room temperature (23 °C) to a target activation temperature of 160 °C at a rate of 2 °C/min in the environmental chamber of the testing machine. This process generated recovery stress in the specimen. The holding time at the activation temperature was 30 min after which the specimen was cooled back to room temperature at 2 °C/min. The specimen was then kept again at room temperature for 30 min before cyclic loading to allow the whole test set up to cool down to room temperature. The remaining recovery stress in the specimen after these 30 min was regarded as the initial recovery stress/pre-stress of the specimen. It is noted that an initial prestrain of 4% was selected in this study following the recommendations of [25], which showed that the optimum level of prestraining for generating the maximum initial recovery stress is 2–4% for Fe-SMA strips.

The non-prestrained specimens were mainly considered to study the inelastic buckling behavior of the as-received (virgin) material. The prestrained non-activated or prestrained activated specimens were not considered for this purpose because initial prestraining and activation

Table 1
Specimen Matrix for Characterization of Cyclic Behavior.

Specimen	Diameter (mm)	Loading	State	Protocol
1	7.5	Cyclic	Prestrained	50 Cycles @ 0.075% Strain Amplitude
2	7.5	Cyclic	Activated@160 °C	50 Cycles @ 0.075% Strain Amplitude
3	7.5	Cyclic	Prestrained	50 Cycles @ 0.15% Strain Amplitude
4	7.5	Cyclic	Activated@160 °C	50 Cycles @ 0.15% Strain Amplitude
5	7.5	Cyclic	Prestrained	50 cycles@0.4% Strain Amplitude
6	7.5	Cyclic	Activated@160 °C	50 cycles@0.4% Strain Amplitude
7	5.25	Cyclic	Prestrained	Incremental Amplitudes (0.03125%, 0.0625%, 0.125%, 0.25%, 0.5%, 1.0%)
8	5.25	Cyclic	Activated@160 °C	Incremental Amplitudes (0.03125%, 0.0625%, 0.125%, 0.25%, 0.5%, 1.0%)
9	5.25	Cyclic	Prestrained	Incremental Amplitudes (0.1%, 0.2%, 0.3%, 0.4%, 0.5%, 0.6%, 0.7%, 0.8%, 0.9%, 1.0%)
10	5.25	Cyclic	Activated@160 °C	Incremental Amplitudes (0.1%, 0.2%, 0.3%, 0.4%, 0.5%, 0.6%, 0.7%, 0.8%, 0.9%, 1.0%)
11	7.5	Monotonic	Non-Prestrained	Compressive loading until fracture – Specimen's L/D = 3
12	7.5	Cyclic	Non-Prestrained	Incremental Amplitudes (0.5%, 1.0%, 1.5%, 2.0%, 2.5%, 3.0%, 3.5%, 4.0%, 4.5%, 5.0%) – Specimen's L/D = 3
13	7.5	Monotonic	Non-Prestrained	Compressive loading until fracture – Specimen's L/D = 4
14	7.5	Cyclic	Non-Prestrained	Incremental Amplitudes (0.5%, 1.0%, 1.5%, 2.0%, 2.5%, 3.0%, 3.5%, 4.0%, 4.5%, 5.0%) – Specimens's L/D = 4
15	10.5	Cyclic	Activated@160 °C	Incremental Amplitudes (0.03125%, 0.0625%, 0.125%, 0.25%, 0.5%, 1.0%)
16	10.5	Cyclic	Heat-Treated and Activated@160 °C	Incremental Amplitudes (0.03125%, 0.0625%, 0.125%, 0.25%, 0.5%, 1.0%)

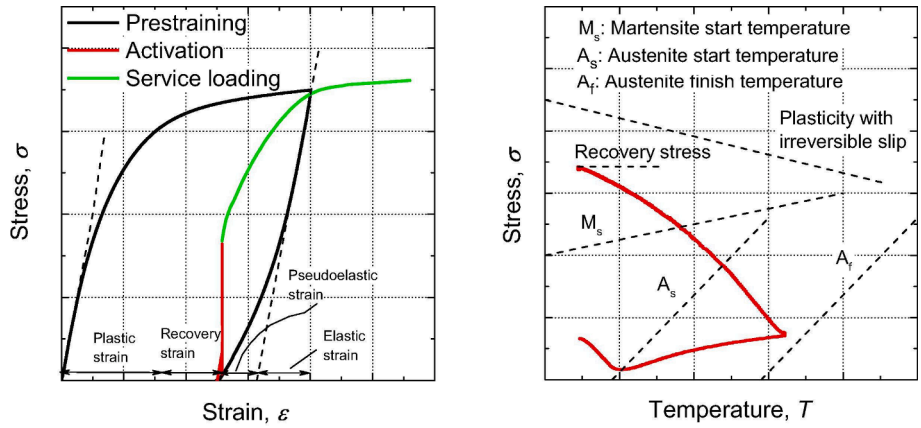

Fig. 2. Thermal activation of Fe-SMA: a) stress-strain characteristics; b) stress-temperature characteristics (Reprinted from [25]).

results in an asymmetry in the tension-compression stress behavior of the Fe-SMA, which makes it difficult to identify the commencement of softening in the compressive behavior of Fe-SMA due to the onset of buckling. The purpose of using prestrained non-activated specimens was two-fold: i) to identify the strain limit when a thermally activated specimen starts behaving identically to a non-activated prestrained specimen after losing its initial pre-stress. ii) to understand the effect of prestraining on the tension-compression asymmetry. Thermally activated prestrained specimens, on the other hand, were used to study the loss in pre-stress under cyclic loading reversals. In addition to the three types of specimens mentioned before (i.e. non-prestrained, prestrained non-activated, and prestrained activated), a heat-treated specimen was also used in the experimental campaign to study the effect of prior heat-treatment on the pre-stress loss behavior. For preparing this specimen, the as-received 10.5 mm diameter rebar was first subjected to heat-treatment of about 750 °C for 6 h in an oven. Later on, the rebar was prestrained and activated using the same procedure mentioned previously. It is noted that for simplicity the prestrained non-activated and prestrained activated specimens will be referred to as prestrained and activated specimens, respectively, throughout the manuscript. Also, the terms recovery stress and pre-stress are used interchangeably.

2.2. Loading protocols

Four types of loading protocols were used in the experimental testing campaign. The loading histories included, constant strain amplitude tension-compression reversals, incremental (small) strain amplitude tension-compression reversals, incremental (large) strain amplitude tension-compression reversals, and monotonic compression. The constant strain amplitude experiments comprised up to 50 tension-compression reversals at a given strain amplitude, whereas the incremental strain amplitude experiments consisted of one cycle of incrementally increasing strains. The constant and incremental (small) strain amplitude tests were mainly conducted to investigate the loss in pre-stress of Fe-SMA under cyclic loading reversals. In these tests, the loading was extensometer-controlled with a strain rate of 0.03%/s. On the other hand, the monotonic compression and incremental (large) strain amplitude tension-compression reversals were used to investigate the inelastic buckling behavior of Fe-SMA under a stroke-controlled loading (to prevent damage to extensometer) at the same strain rate (i.e. 0.03%/s).

2.3. Experimental test setup

The experiments were conducted on a computer-controlled servo-hydraulic Walter + Bai (W&B) machine (Type LFV 500-HH) with a ±100 kN load cell (model: GTM K 100kN) and wedge grips (WGR-100-M Inserts for round specimens with ø 10–16/19 mm). The machine has a piston stroke capacity of ±125 mm which is measured using a displacement transducer type MTS RHM0280MD701S2B8102, NO 1806 323. The machine is equipped with an ultra-high-speed, high-resolution digital material testing control system PCS8000 with remote control. The software program used for operating the machine is DION7. The thermal activation of the specimens was performed in the environmental chamber (Type ETC 460-2) with a temperature range of −80 °C to 300 °C installed with the machine. The chamber has a stainless steel interior with a recirculating fan at its rear and Inconel sheathed heating elements. The chamber is equipped with high-grade insulation and has an integrated control system, based on a type K thermocouple. The temperature controller is a Eurotherm 2216e with an integrated over-temperature alarm to prevent any overheating of the system. For cooling purposes, the chamber is connected to a 120-liter liquid nitrogen container. The details of the experimental test setup are shown in Fig. 3.

An axial extensometer (Type: EXA15-2u S/N 2035) with a gauge

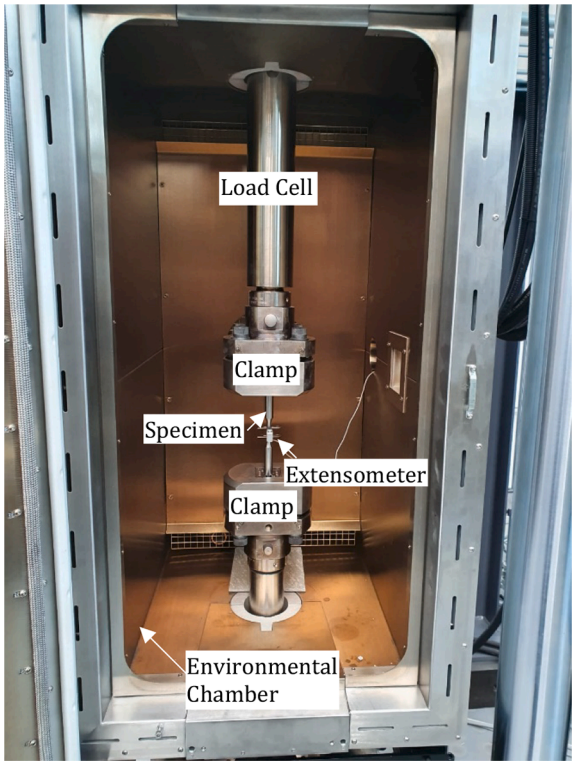

Fig. 3. Experimental test setup.

length of 15 mm was attached for measuring and controlling the deformations in experiments conducted to study the recovery stress behavior of Fe-SMA under cyclic loading. The displacement measuring range of the extensometer was ±2 mm and it could operate in the temperature range from −270 °C up to +300 °C. Based on the extensive calibration tests performed on the extensometer, a control was implemented in the testing machine to continuously compensate for the temperature-induced expansion of the extensometer.

The experiments to investigate the inelastic buckling behavior (specimens 11–14) were stroke-controlled to prevent any damage to the extensometer due to geometric nonlinearity resulting from buckling. Thus, the machine displacement data (without any post-processing) has been used to calculate strains and the measured strains for buckling tests represent the global deformation, including geometric changes due to buckling. All tests were conducted at the ambient temperature in the laboratory.

3. Results and discussion

This section presents the results of the material characterization study where aspects such as loss of the recovery stress under cyclic loading, implications of initial prestraining on the symmetry/asymmetry of the stress-strain behavior of Fe-SMA, and the inelastic buckling behavior of Fe-SMA under monotonic compression and cyclic tension-compression reversals are investigated in detail.

3.1. Effect of cyclic loading on recovery stress

The understanding of the extent of loss in the recovery stress of Fe-SMA under cyclic loading is crucial for seismic design and retrofitting applications. Particularly, the strain limit corresponding to the total loss in the recovery stress when an activated and a prestrained specimen would start behaving similarly should be known for the design purposes. For this purpose, the behavior of activated and prestrained Fe-SMA under constant and incremental strain reversals is compared in this section. The constant strain amplitude experiments were performed on dogbones with reduced section diameter, D = 7.5 mm, whereas incremental strain amplitude experiments were performed on dogbones with D = 5.25 mm. Irrespective of the loading protocol considered, the complete loss of recovery stress for both types of specimens occurred at the same cyclic strain amplitude (i.e. ~ 0.4–0.5%).

3.1.1. Constant strain amplitude experiments

The constant loading tests were conducted at three different strain amplitudes (i.e. ±0.075%, ±0.15%, and ±0.4%). The strain amplitudes were selected to represent the specimen behavior in the early stages of the elastic range (±0.075%), and afterwards (i.e. ±0.15% and ±0.4%). The specimens were divided into three groups where each group consisted of one prestrained and one activated specimen. The first group of specimens (i.e. specimens 1 and 2) was subjected to 50 cycles of ±0.075% strain. The loading history for the second group of specimens (i.e. specimens 3 and 4) was 50 cycles at ±0.15% strain. The last group of specimens (i.e. specimens 5 and 6) was subjected to 15 cycles of ±0.4% strain. The stress-strain behavior of the first, second, and third groups of specimens is shown in Fig. 4(a), (b), and (c), respectively. The initial recovery stress of the activated specimens was 280 MPa for the first group, 260 MPa for the second group, and 280 MPa for the third group, as shown in Table 2. For a fair comparison with the activated specimens that were subjected to an initial preload of 50 MPa before activation, the prestrained specimens were also preloaded to 50 MPa in all cases before cyclic loading.

Fig. 4(a) shows that the loss in the initial recovery stress at ±0.075% strain amplitude was 50 MPa upon unloading from the first cycle. In contrast, the loss upon unloading from the first cycle was 125 MPa at ±0.15% and 275 MPa (i.e. total recovery stress loss) at ±0.4% strain amplitudes, as shown in Fig. 4(b) and (c), respectively. The loss of the recovery stress was minimal in the subsequent cycles, especially for specimens subjected to ±0.075% and ±0.15% strain amplitudes. On the other hand, total loss of the recovery stress occurred after the first two

Table 2
Recovery stress behavior of activated Fe-SMA under constant strain amplitude tests.

Loading Case	Initial Recovery Stress (MPa)	Recovery Stress at Unloading from 1st Cycle (MPa)	Recovery Stress at Unloading from Last Cycle (MPa)
50 cycles @ 0.075% strain (Specimen 2)	280	230	210
50 cycles @ 0.15% strain (Specimen 4)	260	135	120
15 cycles @ 0.4% strain (Specimen 6)	280	5	0

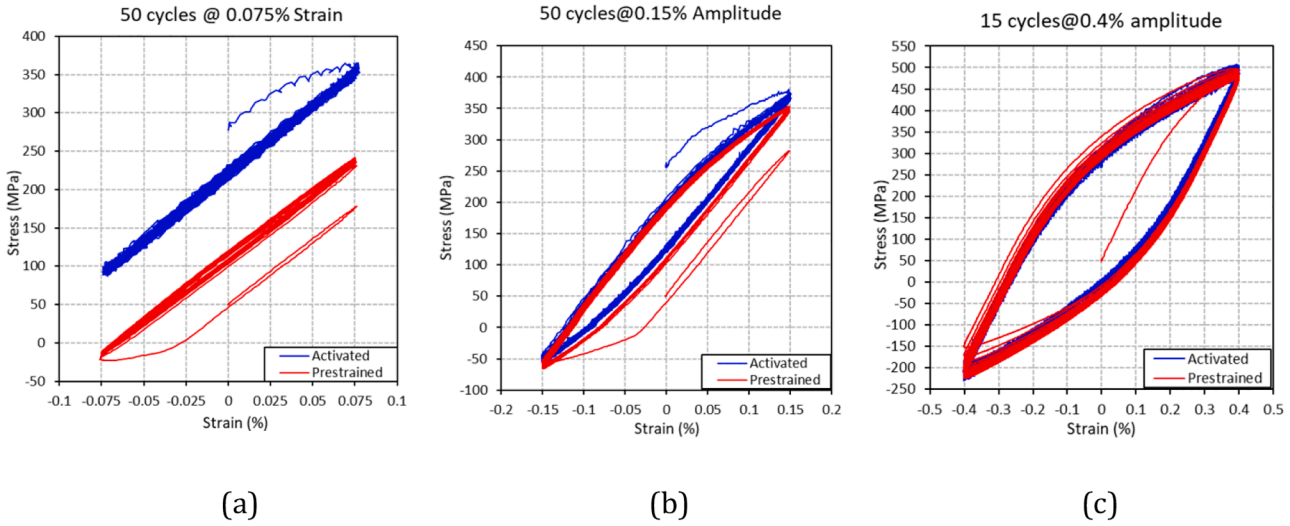

Fig. 4. Loss of recovery stress under constant strain amplitude: a) 50 cycles@0.075% strain (Specimens 1 and 2); b) 50 cycles@0.15% strain (Specimens 3 and 4); c) 15 cycles@0.4% strain (Specimens 5 and 6).

cycles at ±0.4% strain amplitude. That's why 15 cycles (instead of 50 cycles) were used at ±0.4% amplitude, as the recovery stress was already lost.

The results in Fig. 4 indicate that the stress-strain behavior of activated and the prestrained specimens approach each other with the increase in the strain amplitude and become similar after the complete loss of pre-stress (refer Fig. 4(c)). This has important implications from the design point of view. It implies that after the strain limit corresponding to the total loss of the recovery stress, an activated Fe-SMA rebar will behave similarly to a non-activated prestrained Fe-SMA rebar.

Fig. 4(a) shows that the slope of the stress-strain curve in the first loading cycle after activation is smaller than the rest of the loading cycles. Infact, the specimen exhibited a linear elastic behavior in all the subsequent loading cycles. Similar behavior was observed in [27], where Fe-SMA specimens were tested under high-cycle fatigue loading. It is possible that the change in slope in the first loading cycle after activation is related to the initial level of prestraining but this needs to be ascertained with more tests in future where activated specimens with different levels of initial prestraining are subjected to cyclic loading reversals. In a previous study by Shahverdi et al.[25], it was shown that the slope after activation depends on the activation temperature. As such, among the considered activation temperatures of 120 °C, 160 °C and 195 °C, the maximum slope on loading after activation was exhibited by the specimen activated at 195 °C. Further studies on microstructural behavior might help in understanding the reasons for this behavior.

Interestingly, a closer look at Fig. 4(b) reveals two different stiffnesses during the first cycle of loading of the activated specimen. The stiffness seems to change after 0.025% strain amplitude, which corresponds to additional stress of around 50 MPa after activation. It is possible that the loss in recovery stress of Fe-SMA under cyclic loading starts from this point of change in stiffness; however, this needs to be investigated further.

3.1.2. *Incremental strain amplitude experiments*

Two different incremental strain histories were used to study the loss of recovery stress. Specimens 7 and 8 were subjected to incremental strain history with the following amplitudes: ±0.03125%, ±0.0625%, ±0.125%, ±0.25%, ±0.5%, and ±1%, as shown in Fig. 5. In contrast, specimens 9 and 10 were tested under incremental strain amplitudes of ±0.1%, ±0.2%, ±0.3%, ±0.4%, ±0.5%, ±0.6%, ±0.7%, ±0.8%, ±0.9%, ±1.0%, as shown in Fig. 6. The purpose of using two load histories with different increments was to evaluate the effect of loading history on the strain limit associated with the complete loss of pre-stress.

Fig. 5 (a-d) and Table 3 indicate that the initial recovery stress of 300 MPa in the activated specimen reduced by 20 MPa, 50 MPa, 110 MPa,

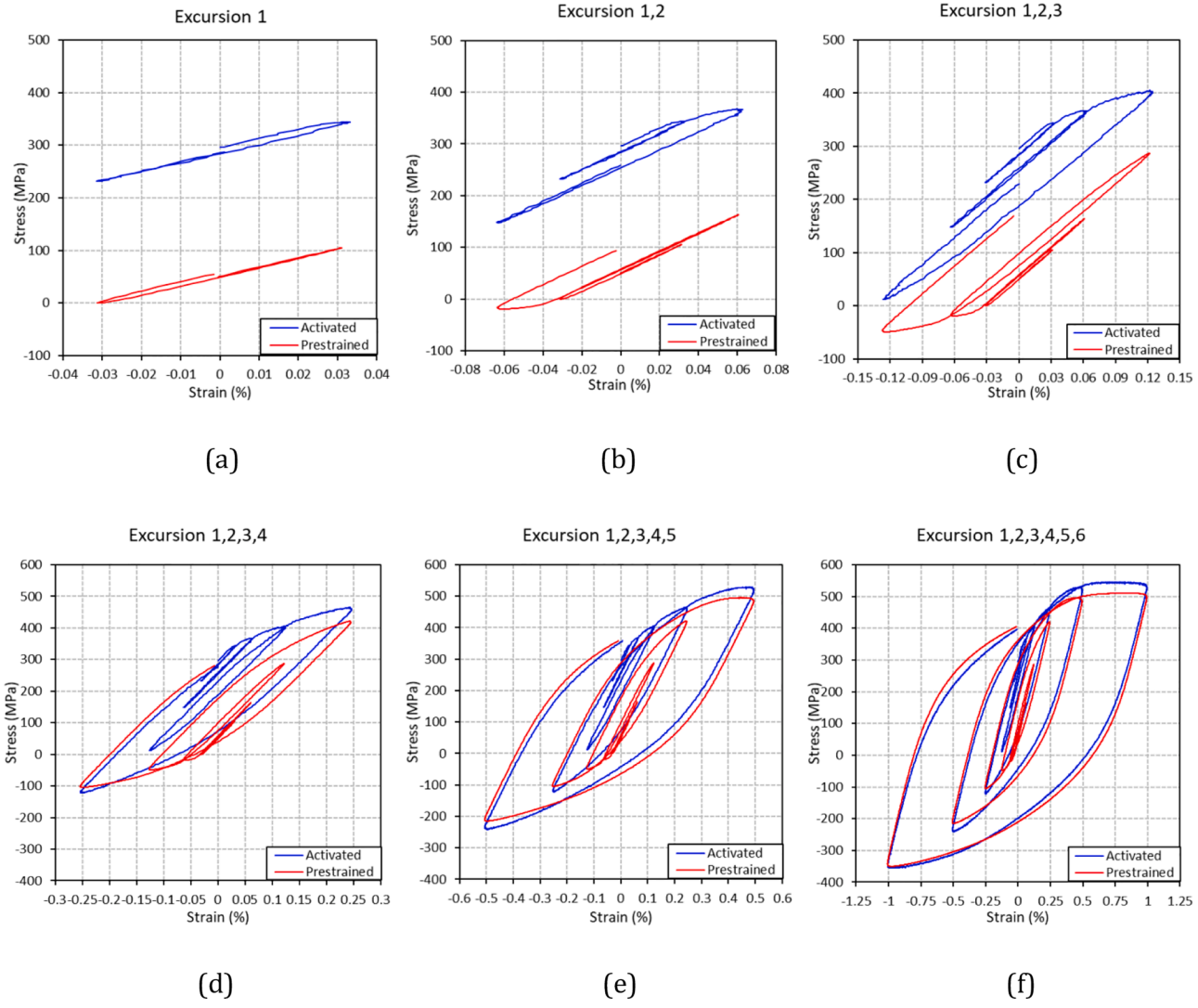

Fig. 5. Loss of recovery stress under incremental strain amplitude (Specimen 7 and 8): a) ±0.03125% strain amplitude; b) ±0.0625% strain amplitude; c) ±0.125% strain amplitude; d) ±0.25% strain amplitude; e) ±0.5% strain amplitude; f) ±1.0% strain amplitude.

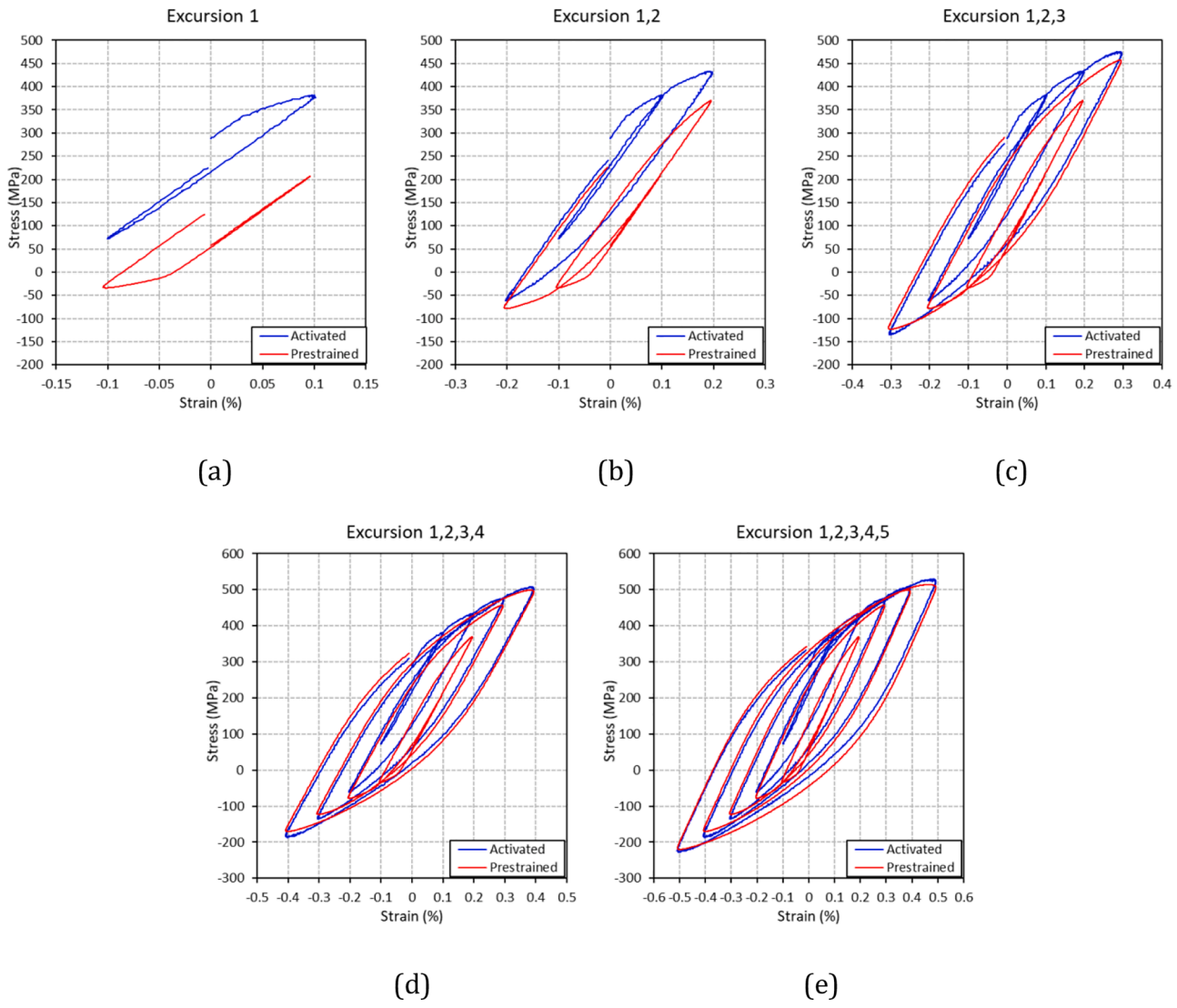

Fig. 6. Loss of recovery stress under incremental strain amplitude (Specimen 9 and 10): a) ±0.1% strain amplitude; b) ±0.2% strain amplitude; c) ±0.3% strain amplitude; d) ±0.4% strain amplitude; e) ±0.5% strain amplitude.

Table 3
Recovery stress behavior of activated Fe-SMA under incremental strain amplitude tests.

Case 1: Specimen 8 – Strains: 0.03125–0.5% Intial Recovery Stress = 300 MPa		Case 2: Specimen 10 – Strains: 0.1–0.5% Initial Recovery Stress = 290 MPa	
Strain Amplitude (%)	Recovery Stress at Unloading (MPa)	Strain Amplitude (%)	Recovery Stress at Unloading (MPa)
0.03125	280	0.1	220
0.0625	250	0.2	120
0.125	190	0.3	60
0.25	80	0.4	20
0.5	0	0.5	0

and 220 MPa at strain amplitudes ±0.03125%, ±0.0625%, ±0.125%, and ±0.25%, respectively. Fig. 5 (e-f) show that upon unloading from the tension-compression reversals associated with the strain amplitudes of ±0.5% and ±1%, the activated and prestrained specimens exhibited similar stresses. This implies a total loss of the initial recovery stress in the activated specimen. It can be noticed in Fig. 5 that the hysteretic stress-strain behavior of the prestrained and activated specimens is different in the first few excursions and becomes quite similar after the 4th excursion. This is because, during the first few loading excursions, a significant amount of recovery stress is present in the activated specimen. However, after the 4th loading excursion (0.4–0.5%), the recovery stress in the activated specimen is completely lost and thereafter the activated specimen behaves similarly to a non-activated prestrained specimen, as evident in Fig. 5(e) and (f). Similar results in terms of loss in recovery stress were obtained when the same experiment was repeated on a 10.5 diameter rebar specimen (specimen 15), confirming that the recovery stress loss behavior of dogbone specimens is similar to the rebars from which they are manufactured.

Fig. 6 and Table 3 show that the specimens subjected to constant strain increments of ±0.1% experienced loss of around 70 MPa, 170 MPa, 230 MPa, and 270 MPa in the initial recovery stress of 290 MPa at the strain amplitudes of ±0.1%, ±0.2%, ±0.3%, and ±0.4%, respectively. At ±0.5% strain amplitude, the recovery stress was lost completely and the activated specimen once again exhibited similar stress-strain hysteretic behavior to that of the prestrained non-activated specimen. The comparison of results from Figs. 5 and 6 show that the loss of recovery stress is dependent on the strain amplitude and is independent of the increments. This can be concluded because a similar loss is observed for similar strain amplitudes in these two different experiments.

3.1.3. Relationship between loss in recovery stress and recovered strains

It is clear from the stress-strain behavior of activated Fe-SMA specimen under constant and incremental strain amplitudes that the total loss of the recovery stress occurs when the strain amplitude is 0.4–0.5%. This strain limit is not arbitrary rather it seems to be equal to the recovered strains (i.e. pseudoelastic and elastic strain recovered) after initial prestraining of Fe-SMA, as shown in Fig. 7 (a). The pseudoelastic strain is the strain that recovers nonlinearly upon unloading. It is noted that for an initial prestrain of 4%, the recovered elastic strains were in the range of 0.25–0.30%, whereas the pseudoelastic strains were in the range of 0.15–0.20%. The stress-strain behavior of Fe-SMA specimen for the three stages i.e. initial prestraining, followed by activation, and cyclic loading reversals, shown in Fig. 7 (b), confirms this observation. The enlarged view of the stress-strain behavior for the activation and cyclic loading stages shown in Fig. 7 (c) provides a more clear picture of the dependence of the strain limit associated with the total loss of the recovery stress on the recovered strains after initial prestraining. The figure shows that under cyclic loading after activation, as soon as the total strain reaches the initial prestrain, there is total loss of the recovery stress and the specimen goes into compression. This implies that the available strain limit within which the recovery stress under cyclic loading would be lost partially is slightly less than the recovered strains after initial prestraining. Other specimens tested under different constant and incremental strain histories exhibited the same behavior in terms of the dependence of strain limit associated with the total loss of recovery stress on the recovered strains after initial prestraining. For instance, Fig. 7 (d) shows that the specimen 10 that was tested under incremental strain amplitudes of 0.1–0.5% completely loses its recovery stress under cyclic loading once the total strain after activation reaches the initial prestrain. Similarly, Fig. 7 (e) shows that specimen 6 which was subjected to 15 cycles of 0.4% strain (constant strain amplitude) retains only 5 MPa of recovery stress upon unloading from the first cycle. This is because the total strain in the specimen is slightly less than the initial prestrain. These findings indicate that irrespective of the specimen size (D = 7.5 mm or 5.25 mm) and loading protocol, the phenomenon governing the complete loss of pre-stress under cyclic loading is the same. This phenomenon, as mentioned before, is that the complete loss of initial pre-stress occurs when the cyclic strain amplitude exceeds the total recovered strains obtained after the initial prestraining of the Fe-SMA. It should be noted, however, that the slight difference in behavior between the dogbone specimen sizes was observed in terms of the initial recovery stress generated, which was a bit higher (10–20

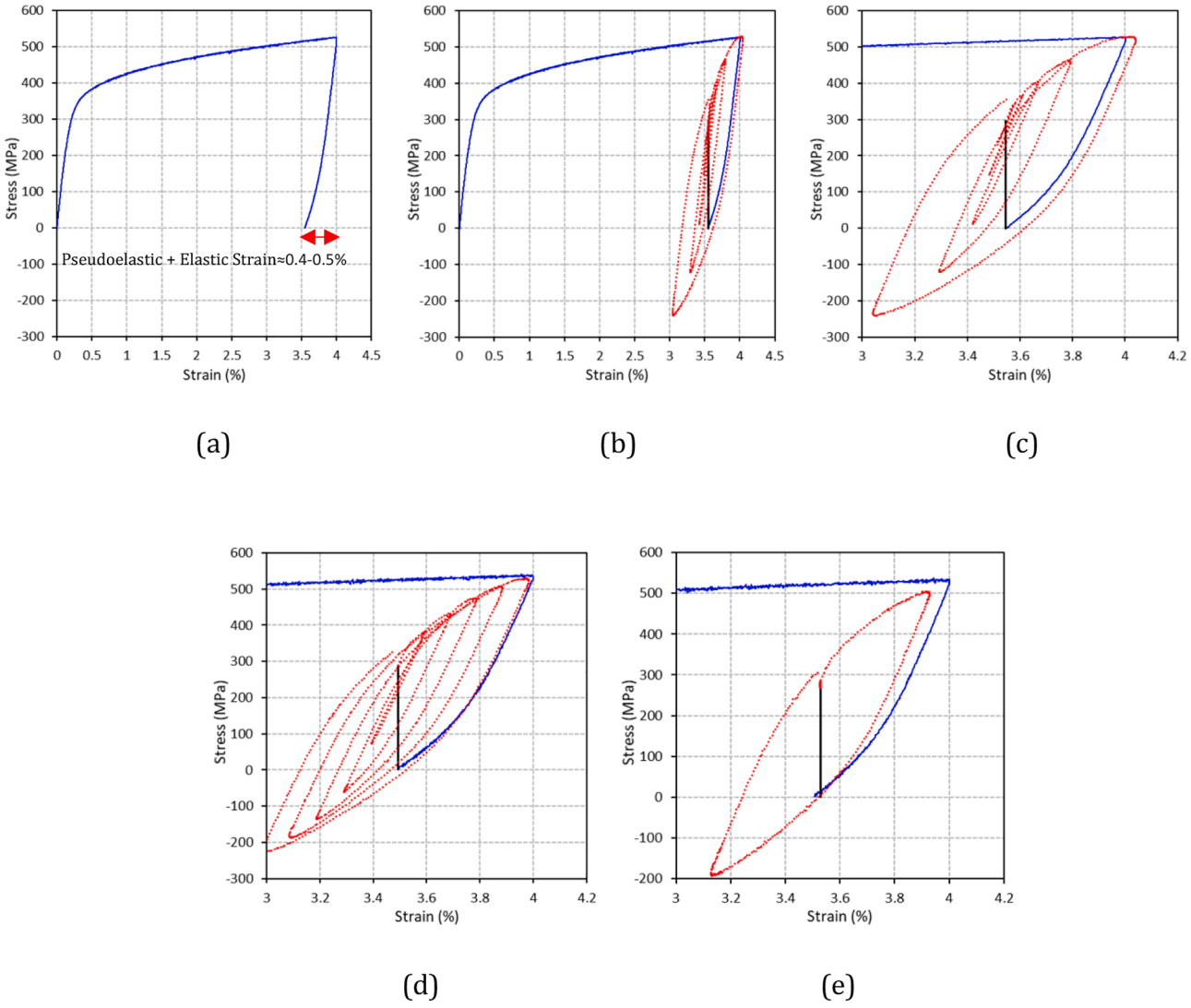

Fig. 7. Dependence of loss in recovery stress on recovered strains after initial prestraining: a) specimen 8: initial prestraining to 4%; b) specimen 8: incremental amplitude cyclic loading after activation (strain amplitudes: 0.03–0.5%); c) specimen 8: incremental amplitude cyclic loading after activation enlarged view (strain amplitudes: 0.03–0.5%); d) specimen 10: incremental amplitude cyclic loading after activation enlarged view (strain amplitudes: 0.1–0.5%); e) specimen 6: constant amplitude cyclic loading after activation enlarged view of first cycle (strain amplitude: 0.4%).

MPa) for dogbone with 5.25 mm diameter.

In the past, similar findings have been reported about the behavior of pre-stressed Ni-Ti-Nb SMA wire, which also experienced total loss of the pre-stress under cyclic loading once the total strain on loading after activation was equal to the initial prestrain [33–35]. Choi et al. [33] concluded that under cyclic loading after activation, Ni-Ti-Nb SMA wires act like a viscoelastic spring from the point of recovered strains (after initial prestraining) to the initial prestrain. This is because no additional strain develops in the material within this strain limit under cyclic loading. On the other hand, residual strains start accumulating in the material once this strain limit is exceeded. This similar behavior can also be observed for Fe-SMA specimens tested in this study, which behaved like a viscoelastic spring from the point of recovered strains (after initial prestraining) to the initial prestrain. The reason for this behavior is that no residual strain accumulates in the Fe-SMA material within this strain limit, as it can be seen in Fig. 7 (c) that the specimen successfully unloads to zero strain in this range. However, as soon as this strain limit is exceeded, the residual strain starts accumulating and the material enters into the plastic phase, thereby completely losing its recovery stress. Fig. 7(c) shows the accumulation of residual strain in the specimen after the initial prestrain of 4% is exceeded.

These findings suggest that the available strain limit of the Fe-SMA in which recovery stress is partially retained can be increased by increasing the pseudoelasticity of the Fe-SMA material. Previous research has shown that the Fe-SMA rebars can be subjected to ageing and heat treatment to increase their pseudoelasticity. For instance, Yang et al. [36] observed a 100% increase in the pseudoelastic strain of Fe-SMA when it was subjected to heat treatment at 774 ^{O}C for 144 hrs. However, prior to the heat treatment, these specimens were solutionized at 1070 ^{O}C for 2 hrs and then quenched in water. More recent investigations at Empa have shown that the heat treatment and ageing without solutionizing may result in a greater increase in the pseudoelastic strains of Fe-SMA. As such, pseudoelastic strains of up to 0.9% could be obtained upon heat treatment at 750 ^{O}C for 6 hrs.

To verify this assertion, 10.5 mm Fe-SMA rebar specimens were subjected to the aforementioned heat treatment at 750 ^{O}C for 6 hrs. These additional rebar specimens were then prestrained, activated at 160 ^{O}C, and subsequently subjected to incremental cyclic loading. The total recovered strain obtained upon initial prestraining of the specimens increased to about 1.25%, as shown in Fig. 8 (a). After thermal activation, the specimens were subjected to tension-compression reversals with strain amplitudes ±0.03125%, ±0.0625%, ±0.125%, ±0.25%, ±0.5%, and ±1.0%. Fig. 8 (b) shows that upon unloading from 0.5% strain amplitude, the heat-treated specimen retained recovery stress of about 150 MPa, whereas previously, the testing of the as-received material (without heat treatment) has shown a total loss of the recovery stress at 0.5% strain amplitude. Similarly, upon unloading from 1% strain amplitude, the heat-treated specimen retained recovery stress of 20 MPa as opposed to the as-received specimens that experienced compression at this strain due to total loss of the recovery stress. This implies that the available strain limit for the recovery stress of Fe-SMA under cyclic loading can be increased from 0.4-0.5% to about 1.25% by heat treatment and ageing of the as-received material at 750 ^{O}C for 6 hrs. The elastic modulus of the Fe-SMA reduced by about 10–20 GPa upon heat treatment.

It should be noted, however, that heat treatment and ageing can reduce the ductility of the material. For instance, the tensile loading on the as-received and heat-treated specimen showed that the failure strain of the material reduced from about 32% to 8% upon heat treatment. According to the requirements of Eurocode 2 [40], the minimum allowable characteristic strain at maximum force is 2.5% and 7.5% for steel rebars and decoiled rods of class A and C, respectively. This implies that Fe-SMA rebar exhibits an adequate failure strain (i.e. 8%) even after heat treatment and ageing and can still be used for structural applications. Another good alternative for improving the pseudoelasticity of Fe-SMA can be to increase the initial prestraining level. Past studies [25,27] have shown that at a higher initial prestrain Fe-SMA exhibits a larger pseudoelastic strain. Similarly, a recent study [38] has shown that additive manufacturing using the laser powder bed fusion method can enhance the shape memory effect and pseudoelasticity of Fe-SMA compared to the conventional fabrication methods [38]. All these aspects show that the pre-stressed Fe-SMA has a promising potential for seismic design and retrofitting applications; however, its recovery stress properties need to be optimized.

3.2. *Effect of prestraining on cyclic behavior*

Since Fe-SMA rebars are mostly supplied in the prestrained form (usually 4%) for construction applications, so it is important to understand the effect of the prestraining on the stress-strain behavior, particularly under tension-compression reversals. This effect can be understood from Figs. 4-6, where a significant nonlinearity can be observed as soon as the stress in the prestrained rebar enters the compression regime. This highly asymmetric tension-compression behavior of the prestrained specimen is in contrast with the behavior of non-prestrained specimen, which exhibits quite symmetric behavior

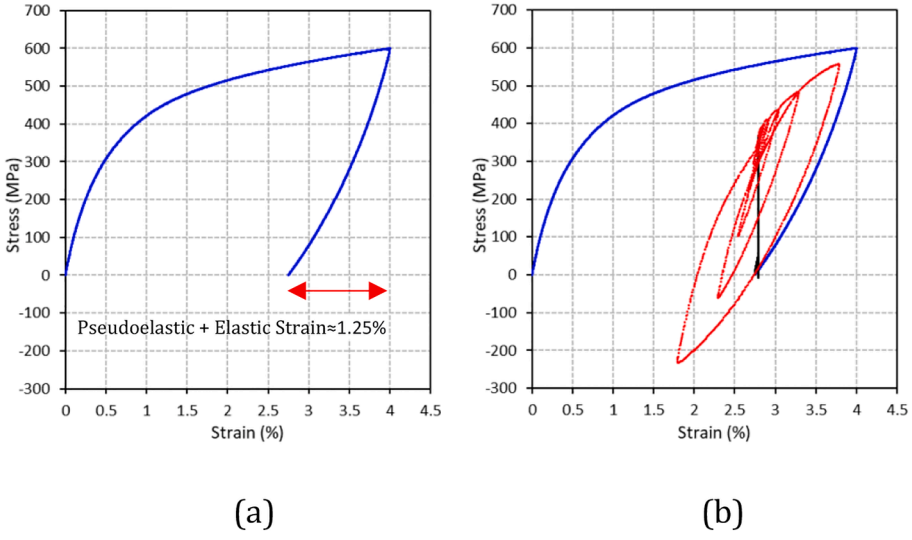

Fig. 8. Effect of heat treatment (750 °C) and ageing (6 hrs) on the loss of recovery stress of Fe-SMA rebar (D = 10.5 mm) under cyclic loading: a) initial prestraining to 4%; b) cyclic loading after activation.

(in terms of maximum tensile/compressive stress) until the commencement of buckling, as shown in Fig. 9. In short, a prestrained specimen exhibits reduced stiffness and highly nonlinear behavior in the compression zone. This aspect should be taken into account when prestrained Fe-SMA (either activated or non-activated) is being used for seismic design applications because, under seismic actions, the structure is being subjected to tension-compression reversals. The asymmetry in tension-compression would imply that RC columns or walls reinforced with prestrained Fe-SMA rebars may experience more damage on the compression face than the tension face. The asymmetry in the stress-strain behavior also needs to be taken into account for the accurate moment-curvature analysis of the cross-sections reinforced with prestrained Fe-SMA rebars. The tension-compression asymmetry of Fe-SMA due to initial prestraining creates a limitation for its use in seismic applications in contrast with conventional steel reinforcement, which exhibits a quite symmetric tension-compression behavior.

3.3. Inelastic buckling behavior

Inelastic buckling occurs when the critical buckling load estimated by the elastic analysis exceeds the yield strength of the material. As a result, this type of buckling happens in the post-yield range of the material and results in the softening of the behavior in the compression regime. The understanding of the inelastic buckling behavior of Fe-SMA rebars under tension-compression reversals is crucial for seismic design and retrofitting applications, particularly in vertical load-bearing

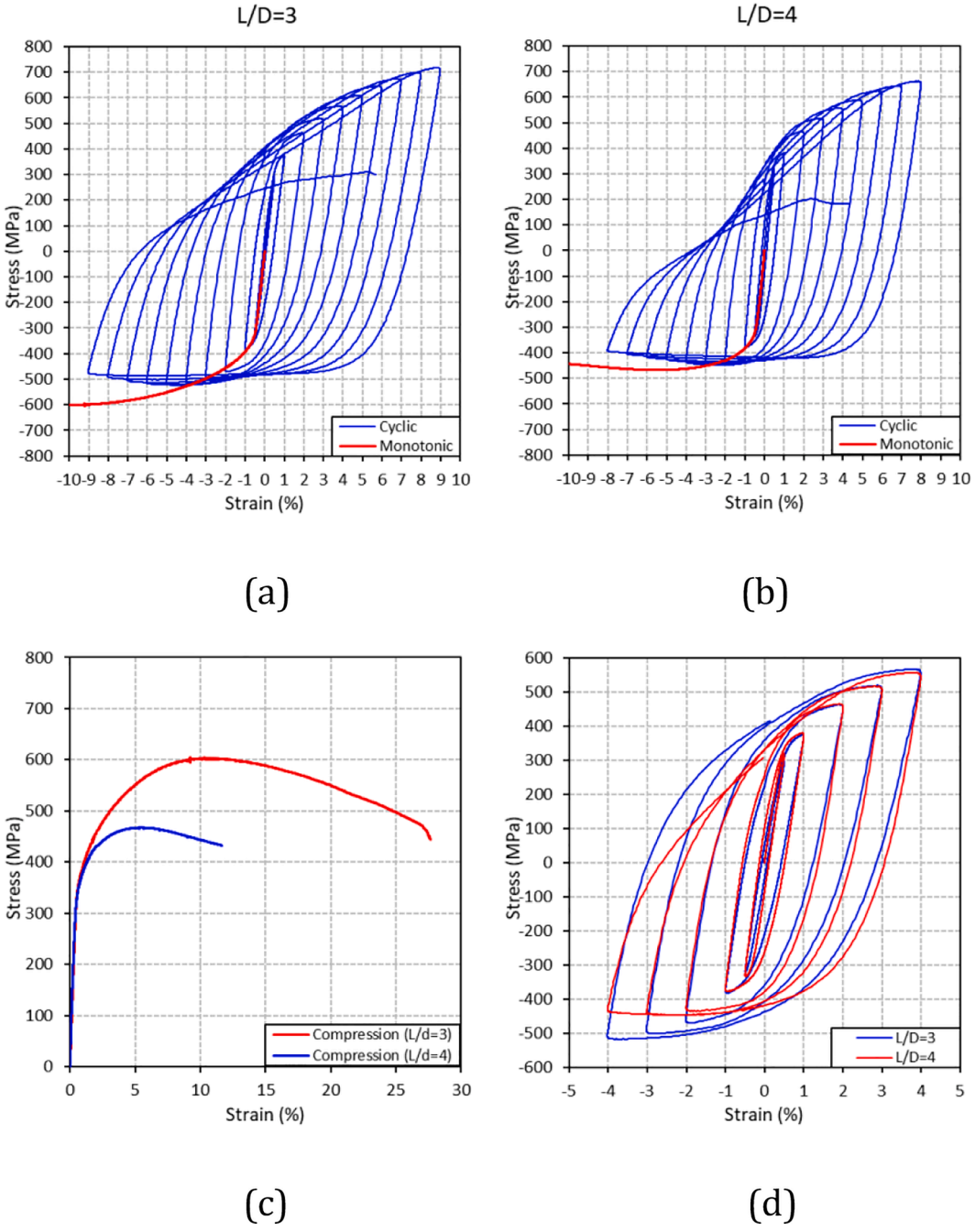

Fig. 9. Stress-strain behavior of Fe-SMA under a) monotonic compression and tension-compression cyclic reversals for L/D = 3 (Specimen 11 and 12); b) monotonic compression and tension-compression cyclic reversals for L/D = 4 (Specimen 13 and 14); c) monotonic compression for L/D = 3 and L/D = 4 (Specimen 11 and 13); d) tension-compression cyclic reversals up to 4% strain for L/D = 3 and 4 (Specimen 12 and 14).

elements (columns, walls). In reinforced concrete elements designed according to the current standards, the design requirements for tie/spiral spacing generally result in the ratio of the unsupported length to the diameter (L/D) of the longitudinal reinforcement between 2.5 and 8 [32]. Considering this, the buckling behavior of Fe-SMA was studied under monotonic compressive and cyclic tension-compression reversals for L/D = 3 and 4, as shown in Fig. 9.

Fig. 9 (a) shows that for L/D = 3, the monotonic and cyclic stress in the compression zone is similar until 4% strain amplitude. With the further increase in the strain amplitude, the stress under cyclic loading gradually decreased (softening) due to buckling until fracture occurred at 9% strain, whereas no decrease in the compressive stress was observed under monotonic loading until 10% strain amplitude. On the other hand, the compressive stress for L/D = 4 was similar under monotonic and cyclic loading until 3% strain amplitude, as shown in Fig. 9 (b). After 3% strain amplitude, the compressive stress under cyclic loading started decreasing due to buckling. The fracture, in this case, occurred at 8% strain amplitude. This shows that the effect of inelastic buckling is more pronounced under cyclic stress-strain reversals as opposed to monotonic compressive loading.

The monotonic compressive behavior for the two L/D values is compared in Fig. 9 (c). It can be observed that the maximum compressive stress in the specimen with L/D = 4 is 80% of the maximum compressive stress in the specimen with L/D = 3. In the specimen with L/D = 4, the maximum compressive stress of about 470 MPa was attained, whereas in the specimen with L/D = 3, a higher maximum compressive stress of 600 MPa was achieved, thereafter the softening in the compressive strength commenced. Since the ultimate tensile strength of Fe-SMA is around 750 MPa and the decrease of L/D from 4 to 3 led to an increase in the ultimate compressive stress by 130 MPa, so it can be expected that a further decrease in L/D of Fe-SMA from 3 to 2 may lead to identical ultimate compressive and tensile strengths. This hypothesis is also supported by the findings in [26], in which Fe-SMA specimens with L/D = 2 were tested under tension-compression reversals of up to 5% strain and didn't experience any buckling.

In Fig. 9 (d), the hysteresis for specimen with L/D = 3 is overlayed with that for the specimen with L/D = 4. It can be noticed that while the two specimens exhibited quite similar hysteretic behavior in the tension regime, the compressive behavior of L/D = 4 deviated from that of L/D = 3 at 2% compressive strain. This deviation became more prominent from 3% strain and onwards. Due to the initiation of buckling, the maximum compressive stresses at 3% and 4% compressive strains were similar to that at 2% strain. The specimen with L/D = 4 experienced a significant reduction in the hysteretic area due to the softening behavior after the commencement of buckling. The specimen with L/D = 3, on the other hand, exhibited a comparatively larger hysteretic area due to the less pronounced buckling. An interesting aspect is that the fracture of L/D = 3 and L/D = 4 specimens occurred at 9% and 8% strains, respectively, despite the initiation of buckling at 3–4 times smaller strain values.

To provide a better perspective on the buckling behavior of SMAs, the study by Barceló and Bonet [41] on the monotonic compression behavior of Ni-Ti SMA rebars with L/D = 6, 9.5, 12, 16.5, 20.5, and 27 is discussed herein. The results of this study showed that the instability in compression for L/D = 6, 9, and 12 commenced at a compressive stress of 470 MPa, irrespective of the L/D ratio. This was mainly attributed to the material transformation to the martensitic phase at a compressive stress of 470 MPa and the associated decrease in the elastic modulus due to this transformation (i.e. from about 65 GPa to 28 GPa). On the other hand, the onset of buckling occurred in the austenite phase at much smaller stresses for L/D = 16.5, 20.5, and 27. The comparison of the cited study with the present study indicates that the superelastic Ni-Ti SMA rebars tend to exhibit better resistance to buckling than the Fe-SMA rebars considered in this study. This may be because the cited study showed that in the absence of buckling, the Ni-Ti rebars can reach very high ultimate compressive stresses and strains of up to 2000 MPa and 130%, respectively. In contrast, the ultimate tensile stresses and strains of Ni-Ti rebars were reported to be 800 MPa and 140%, respectively

3.4. Comparison with steel rebars

Fe-SMA rebars offer certain advantages and a few disadvantages over conventional steel reinforcement. The biggest advantage is that they possess a unique self-prestressing ability upon thermal activation, which the conventional steel rebars lack. As such, the recovery stress of about 300 MPa can be generated upon activation of a single Fe-SMA rebar, which has the same ribbed geometry as conventional steel rebars. This pre-stressing ability can be particularly useful for structural elements, such as beams, columns, walls, and beam-column joints that are expected to experience low and high-cycle fatigue loading. In addition, the Fe-SMA rebars are very ductile and exhibit a fracture strain of over 30% in the absence of buckling and over 8% in the case of inelastic buckling when L/D is 3 and 4. On the other hand, the requirement for conventional steel rebars of classes A, B, and C is to exhibit a minimum fracture strain of 2.5, 5.0, and 7.5%, respectively [40]. This means that Fe-SMA rebars meet the ductility requirements quite well. Furthermore, the elastic modulus of the as-received (non-prestrained) Fe-SMA rebars (calculated between 20 and 200 MPa) used in this study was found to be in the range of 180–185 GPa, which is quite close to the elastic modulus of conventional steel (i.e. 200 GPa). However, the elastic modulus of Fe-SMA reduces significantly upon thermal activation and was found to be in the range of 75–85 GPa after activation. The yield and ultimate strengths of the non-prestrained Fe-SMA are about 400 MPa and 800 MPa, respectively, which indicates an average ratio of 2 between these strengths. On the other hand, the minimum ratio between yield and ultimate strengths is recommended to be 1.05, 1.08 and 1.15, for the steel rebars of classes A, B and C, respectively. It should be noted that the yield strength of the aforementioned steel rebars is in the range of 400–600 MPa [40].

The Fe-SMA reinforcement exhibits pseudoelasticity upon unloading, whereas conventional steel rebars do not show pseudoelasticity. Furthermore, the pseudoelasticity of Fe-SMA can be enhanced by alloy treatments, including heat treatment and ageing. The pseudoelastic strain of Fe-SMA also increases with the increase in the initial prestrain. The limitation of prestrained and activated Fe-SMA rebars, compared to steel rebars, is the asymmetric tension-compression behavior, which is introduced in the material due to initial prestraining.

In the past studies, the strain at the onset of buckling of steel rebars was observed to be 3% for L/D = 5 under cyclic loading [32]. For Fe-SMA, the strain at the onset of buckling under cyclic loading is observed to be 2% for L/D = 4 and 3% for L/D = 3. This means that buckling commences earlier in Fe-SMA rebars as compared to steel rebars, which may be attributed to the relatively lower elastic modulus of non-prestrained Fe-SMA (180–185 GPa) than steel (200 GPa). The design implication of this would be to use lower tie spacings for Fe-SMA rebars than steel in seismic design and retrofitting applications.

In the study conducted by Rosa et al. [26], the cyclic behavior of non-prestrained Fe-SMA rebars was compared with structural steels. It was reported that the energy dissipation of Fe-SMA per loading excursion is similar to the structural steel S355J2 + N at small strains. In contrast, at a large strain of 5%, the normalized energy dissipation of Fe-SMA was reported to be about 35% smaller than S355J2 + N. However, Fe-SMA exhibits a comparatively higher hardening response and as a result, can store higher elastic strain energy than structural steels. The study also noted an asymmetry in the tension-compression behavior of Fe-SMA up to a strain amplitude of 2% in the absence of buckling. This asymmetry was in the form of three different tangent moduli observed when the specimen was loaded in compression. The cited study reported that the cyclic hardening/softening response of Fe-SMA is dependent on the strain rate. As such, an increase of about 50 MPa in tensile and compressive stress was observed at slow and intermediate strain rates of

0.03%/s and 0.8%/s, whereas a tension and compression softening of about 50 MPa was observed at a higher strain of 8%/s.

4. Guidelines for the use of Fe-SMA rebars in existing and new RC structures

For the use of Fe-SMA in existing and new structures that are expected to experience cyclic loading (e.g seismic actions), it is important to understand the strain threshold at which the pre-stress is lost completely. The results of this study indicate that for the as-received SMA rebar prestrained up to 4% and then activated at 160 °C, the total loss of pre-stress occurs at the strain amplitude of 0.4–0.5%. This implies that as-received Fe-SMA could be used as pre-stressed reinforcement for situations where pre-stress is required only at the service load level (i.e. for high-cycle fatigue loading scenarios). On the other hand, for seismic applications where pre-stress is required at the ultimate limit state, the available strain limit for recovery stress can be increased by the heat treatment and ageing of Fe-SMA at 750 °C for 6 hrs. However, it should be noted that this can reduce the failure strain of the material to about 8%. Alternatively, the as-received Fe-SMA rebars can be used as unbonded pre-stressed reinforcement instead of bonded pre-stressed reinforcement to delay the loss of the recovery stress. Partial bonding strategies can also be adopted if corrosion concerns arise due to the unbonding of the reinforcement. For instance, SMA rebars with threaded end region and plain middle region can be employed for pre-stressing RC bridge columns for adding a self-centering capability. In such a scenario, the threaded end region will provide adequate anchorage into the foundation, whereas the plain portion of the rebar in the plastic hinge region will delay the loss of the pre-stress due to partial bonding. As a result, the initially applied pre-stress would be able to provide a recentering force to the column even at large drifts. In addition, the partial bonding with concrete will provide corrosion protection. Finally, another alternative could be to retrieve the recovery stress that has been lost under cyclic loading by a second thermal activation of Fe-SMA as previous studies [28] have shown that a thermal reactivation of Fe-SMA can retrieve a significant portion of the recovery stress lost under cyclic loading.

As the experimental results demonstrate that inelastic buckling commences in Fe-SMA slightly earlier than steel, therefore, to delay the onset of buckling at the ultimate limit state, a relatively smaller ratio of unsupported length to the diameter of Fe-SMA rebar should be used as compared to the steel rebars for bonded applications in vertical load-bearing elements. According to EN 1998-2 [37], the maximum spacing limit for steel spirals/ties in RC piers is 5-6d_b for delaying the inelastic buckling of the longitudinal rebars under loading reversals. A similar guideline can be adopted for Fe-SMA rebars by keeping the maximum spacing limit for spirals/ties up to 4d_b to effectively delay the commencement of buckling in the post-yield region. It should be noted, however, that Fe-SMA is mostly used for structural applications in the pre-stressed form. This means that Fe-SMA rebar will be under tensile stresses at the beginning of the cyclic loading. As discussed previously, the total loss in the pre-stress of Fe-SMA rebar is expected at the strain amplitudes of 0.4–0.5%. Thus, rebar will experience compressive stresses beyond these strain amplitudes. So, the spacing of the spiral/tie for preventing buckling of the pre-stressed Fe-SMA rebar should be decided considering the maximum compressive stress that is expected to develop in the Fe-SMA rebars under cyclic loading.

5. Conclusions

This paper presented an experimental investigation into the behavior of pre-stressed Fe-SMA rebars under cyclic loading reversals. The following conclusions can be drawn based on the results of the experiments:

1. The results of the material characterization study under both constant and incremental tension-compression strain reversals indicate that the total loss of the recovery stress/pre-stress of the as-received Fe-SMA rebars occurs at the strain amplitudes of 0.4–0.5%. This strain amplitude limit is not arbitrary, rather it is equal to the total strain recovered (pseudoelastic and elastic strain) upon unloading after initial prestraining of the Fe-SMA rebar.
2. The strain amplitude associated with the total loss of the recovery stress under cyclic loading reversals can be increased by enhancing the pseudoelasticity of the material. This can be achieved by heat treatment and ageing of Fe-SMA. The recovered strains of the as-received Fe-SMA showed an increase from 0.4-0.5% to 1.25% on heat treatment and ageing at 750 °C for 6 hrs. This subsequently also increased the available strain amplitude for retaining the recovery stress of Fe-SMA under cyclic loading to 1.25%.
3. The initial prestraining results in a tension-compression asymmetry of the Fe-SMA rebar. As a result, the rebar exhibits less strength and stiffness in the compressive regime as opposed to the tensile regime. This aspect should be particularly taken into account when pre-strained Fe-SMA is used for seismic design and retrofitting applications because, under seismic actions, the structure is being subjected to tension-compression reversals.
4. The onset of inelastic buckling of Fe-SMA rebars under tension-compression reversals occurs at 4% and 3% strain, respectively, for an unsupported length to diameter ratio (L/D) of 3 and 4. On the other hand, the fracture due to inelastic buckling for these L/D ratios occurs at strains of 9% and 8%, respectively. This implies that rebars with $L/D \leq 4$ possess sufficient resistance to fracture due to inelastic buckling at the serviceability and ultimate limit state. Therefore, it is recommended to limit the unsupported length of Fe-SMA rebar up to 4d_b to effectively delay the commencement of buckling in the post-yield region for applications involving tension-compression reversals.

The present study was the first experimental study which, with a limited number of specimens, attempted to understand the recovery stress loss behavior of Fe-SMA under tension-compression cyclic reversals. More experimental tests are recommended in the future to develop a reliable material behavior model that can account for all variabilities.

CRediT authorship contribution statement

Saim Raza: Conceptualization, Methodology, Investigation, Formal analysis, Writing – original draft. **Julien Michels:** Methodology, Resources, Writing – review & editing. **Moslem Shahverdi:** Conceptualization, Methodology, Writing – review & editing, Supervision, Funding acquisition.

Declaration of Competing Interest

The authors declare that they have no known competing financial interests or personal relationships that could have appeared to influence the work reported in this paper.

Acknowledgments

The financial support from the Swiss Innovation Agency (grant no. 39259.1 IP-ENG) and the technical assistance provided by the Structural Engineering Laboratory staff at Empa is gratefully acknowledged. The authors are also grateful to the industrial partner, re-fer AG, for providing the materials and technical support.

References

[1] A. Cladera, B. Weber, C. Leinenbach, C. Czaderski, M. Shahverdi, M. Motavalli, Iron-based shape memory alloys for civil engineering structures: An overview, Constr. Build. Mater. 63 (2014) 281–293, https://doi.org/10.1016/j.conbuildmat.2014.04.032.

[2] L. Janke, C. Czaderski, M. Motavalli, J. Ruth, Applications of shape memory alloys in civil engineering structures – overview, limits and new ideas, Mater. Struct. 38 (279) (2005) 578–592, https://doi.org/10.1617/14323.

[3] S. Raza, B. Shafei, S. Saiidi, M. Motavalli, M. Shahverdi, Shape Memory Alloy Reinforcement for Strengthening, and Self-Centering of Existing and New RC Structures – State of the Art, Constr. Build. Mater. 324 (2022), https://doi.org/10.1016/j.conbuildmat.2022.126628.

[4] C. Czaderski, M. Shahverdi, R. Brönnimann, C. Leinenbach, M. Motavalli, Feasibility of iron-based shape memory alloy strips for prestressed strengthening of concrete structures, Constr. Build. Mater. 56 (2014) 94–105, https://doi.org/10.1016/j.conbuildmat.2014.01.069.

[5] M. Shahverdi, C. Czaderski, M. Motavalli, Iron-based shape memory alloys for prestressed near-surface mounted strengthening of reinforced concrete beams, Constr. Build. Mater. 112 (2016) 28–38, https://doi.org/10.1016/j.conbuildmat.2016.02.174.

[6] M. Shahverdi, C. Czaderski, P. Annen, M. Motavalli, Strengthening of RC beams by iron-based shape memory alloy bars embedded in a shotcrete layer, Eng. Struct. 117 (2016) 263–273, https://doi.org/10.1016/j.engstruct.2016.03.023.

[7] H. Rojob, R. El-Hacha, Self-prestressing using iron-based shape memory alloy for flexural strengthening of reinforced concrete beams, ACI Struct. J. 114 (2) (2017) 523–532, https://doi.org/10.14359/51689455.

[8] R. El-Hacha, H. Rojob, Flexural strengthening of large-scale reinforced concrete beams using near-surface-mounted self-prestressed iron-based shape-memory alloy strips, PCI J. 55–65 (2018), https://doi.org/10.15554/pcij63.6-03.

[9] H. Rojob, R. El-Hacha, Fatigue performance of rc beams strengthened with selfprestressed iron-based shape memory alloys, Eng. Struct. 168 (2018) 35–43, https://doi.org/10.1016/j.engstruct.2018.04.042.

[10] J. Michels, M. Shahverdi, C. Czaderski, Flexural strengthening of structural concrete with iron-based shape memory alloy strips, Struct. Concr. 19 (3) (2018) 876–891, https://doi.org/10.1002/suco.201700120.

[11] K. Hong, S. Lee, Y. Yeon, K. Jung, Flexural response of reinforced concrete beams strengthened with near-surface-mounted fe-based shape-memory alloy strips, Int. J. Concr. Struct. Mater. 12 (1) (2018) 876–891, https://doi.org/10.1002/suco.201700120.

[12] L.A. Montoya-Coronado, J.G. Ruiz-Pinilla, C. Ribas, A. Cladera, Experimental study on shear strengthening of shear critical RC beams using iron-based shape memory alloy strips, Eng. Struct. 200 (2019) 109680, https://doi.org/10.1016/j.engstruct.2019.109680.

[13] E. Strieder, C. Aigner, G. Petautschnig, S. Horn, M. Marcon, M. Schwenn, O. Zeman, P. Castillo, R. Wan-Wendner, K. Bergmeister, Strengthening of reinforced concrete beams with externally mounted sequentially activated iron-based shape memory alloys, Materials 12 (3) (2019) 345, https://doi.org/10.3390/ma12030345.

[14] A. Cladera, L.A. Montoya-Coronado, J.G. Ruiz-Pinilla, C. Ribas, Shear strengthening of slender reinforced concrete t-shaped beams using iron-based shape memory alloy strips, Eng. Struct. 221 (2020) 111018, https://doi.org/10.1016/j.engstruct.2020.111018.

[15] S. Abouali, M. Shahverdi, M. Ghassemieh, M. Motavalli, Nonlinear simulation of reinforced concrete beams retrofitted by near-surface mounted iron-based shape memory alloys, Eng. Struct. 187 (2019) 133–148, https://doi.org/10.1016/j.engstruct.2019.02.060.

[16] N. Dolatabadi, M. Shahverdi, M. Ghassemieh, M. Motavalli, RC Structures Strengthened by an Iron-Based Shape Memory Alloy Embedded in a Shotcrete Layer-Nonlinear Finite Element Modeling, Materials 13 (23) (2020) 5504, https://doi.org/10.3390/ma13235504.

[17] C. Czaderski, M. Shahverdi, J. Michels, Iron based shape memory alloys as shear reinforcement for bridge girders, Constr. Build. Mater. 274 (2021) 121793, https://doi.org/10.1016/j.conbuildmat.2020.121793.

[18] B. Schranz, J. Michels, C. Czaderski, M. Motavalli, T. Vogel, M. Shahverdi, Strengthening and prestressing of bridge decks with ribbed iron-based shape memory alloy bars, Eng. Struct. 241 (2021) 112467, https://doi.org/10.1016/j.engstruct.2021.112467.

[19] M. Rezapour, M. Ghassemieh, M. Motavalli, M. Shahverdi, Numerical Modeling of Unreinforced Masonry Walls Strengthened with Fe-Based Shape Memory Alloy Strips, Materials 14 (11) (2021) 2961, https://doi.org/10.3390/ma14112961.

[20] B. Schranz, C. Czaderski, T. Vogel, M. Shahverdi, Bond behaviour of ribbed near-surface-mounted iron-based shape memory alloy bars with short bond lengths, Mater. Des. 191 (2020) 108647, https://doi.org/10.1016/j.matdes.2020.108647.

[21] B. Schranz, C. Czaderski, T. Vogel, M. Shahverdi, Bond investigations of pre-stressed, near-surface-mounted, ribbed memory-steel bars with full bond length, Mater. Des. 196 (2020) 109145, https://doi.org/10.1016/j.matdes.2020.109145.

[22] B. Schranz, M.F. Nunes, C. Czaderski, M. Shahverdi, Fibre optic strain measurements for bond modelling of pre-stressed near-surface-mounted iron-based shape memory alloy bars, Constr. Build. Mater. 288 (2021) 123102, https://doi.org/10.1016/j.conbuildmat.2021.123102.

[23] E. Ghafoori, M. Neuenschwander, M. Shahverdi, C. Czaderski, M. Fontana, Elevated temperature behavior of an iron-based shape memory alloy used for pre-stressed strengthening of civil structures, Constr. Build. Mater. 211 (2019) 437–452, https://doi.org/10.1016/j.conbuildmat.2019.03.098.

[24] J. Michels, M. Shahverdi, C. Czaderski, R. El-Hacha, Mechanical performance of ironbased shape-memory alloy ribbed bars for concrete pre-stressing, ACI Mater. J. 115 (6) (2018) 877–886, https://doi.org/10.14359/51710959.

[25] M. Shahverdi, J. Michels, C. Czaderski, M. Motavalli, Iron-based shape memory alloy strips for strengthening rc members: Material behavior and characterization, Constr. Build. Mater. 173 (2018) 586–599, https://doi.org/10.1016/j.conbuildmat.2018.04.057.

[26] D.I.H. Rosa, A. Hartloper, A. de Castro e Sousa, D.G. Lignos, M. Motavalli, E. Ghafoori, Experimental behavior of iron-based shape memory alloys under cyclic loading histories, Constr. Build. Mater. 272 (2021) 121712, https://doi.org/10.1016/j.conbuildmat.2020.121712.

[27] E. Ghafoori, E. Hosseini, C. Leinenbach, J. Michels, M. Motavalli, Fatigue behavior of a Fe-Mn-Si shape memory alloy used for pre-stressed strengthening, Mater. Des. 133 (2017) 349–362, https://doi.org/10.1016/j.matdes.2017.07.055.

[28] E. Hosseini, E. Ghafoori, C. Leinenbach, M. Motavalli, S.R. Holdsworth, Stress recovery and cyclic behaviour of an Fe-Mn-Si shape memory alloy after multiple thermal activation, Smart Mater. Struct. 27 (2) (2018) 10, https://doi.org/10.1088/1361-665X/aaa2c9.

[29] S. Bae, M. Mieses Alexa, O. Bayrak, Inelastic Buckling of Reinforcing Bars, J. Struct. Eng. 131 (2) (2005) 314–321, https://doi.org/10.1061/(ASCE)0733-9445(2005)131:2(314).

[30] J.B. Mander, F.D. Panthaki, A. Kasalanati, Low-cycle fatigue behavior of reinforcing steel, J. Mater. Civ. Eng. 6 (4) (1994) 453–468, https://doi.org/10.1061/(ASCE)0899-1561(1994)6:4(453).

[31] G. Monti, C. Nuti, Nonlinear cyclic behavior of reinforcing bars including buckling, J. Struct. Eng. 118 (12) (1992) 3268–3284, https://doi.org/10.1061/(ASCE)0733-9445(1992)118:12(3268).

[32] E. Rodriguez Mario, C. Botero Juan, J. Villa, Cyclic stress-strain behavior of reinforcing steel including effect of buckling, J. Struct. Eng. 125 (6) (1999) 605–612, https://doi.org/10.1061/(ASCE)0733-9445(1999)125:6(605).

[33] E. Choi, H.K. Hong, H.S. Kim, Y.S. Chung, Hysteretic behavior of NiTi and NiTiNb SMA wires under recovery or pre-stressing stress, J. Alloys Compd. 577 (2013) S444–S447, https://doi.org/10.1016/j.jallcom.2012.02.037.

[34] E. Choi, S.-C. Cho, J.W. Hu, T. Park, Y.-S. Chung, Recovery and residual stress of SMA wires and applications for concrete structures, Smart Mater. Struct. 19 (9) (2010) 094013, https://doi.org/10.1088/0964-1726/19/9/094013.

[35] E. Choi, T.-H. Nam, Y.-S. Chung, Y.-W. Kim, S.-Y. Lee, Behavior of NiTiNb SMA wires under recovery stress or pre-stressing, Nanoscale Res. Lett. 7 (1) (2012), https://doi.org/10.1186/1556-276X-7-66.

[36] Y. Yang, A. Arabi-Hashemi, C. Leinenbach, M. Shahverdi, Influence of thermal treatment conditions on recovery stress formation in an FeMnSi-SMA, Mater. Sci. Eng. A 802 (2021) 140694, https://doi.org/10.1016/j.msea.2020.140694.

[37] EN 1998-2 (2005). Eurocode 8: Design of structures for earthquake resistance—Part 2: Bridges. Brussels: European Committee for Standardisation.

[38] I. Ferretto, D. Kim, N.M. Della Ventura, M. Shahverdi, W. Lee, C. Leinenbach, Laser powder bed fusion of a Fe–Mn–Si shape memory alloy, Addit. Manuf. 46 (2021) 102071, https://doi.org/10.1016/j.addma.2021.102071.

[39] ASTM (2019). Standard test method for strain-controlled fatigue testing, American Society for Testing and Materials, West Conshohocken, PA, ASTM No. E606/E606M-19.

[40] EN 1992-1-1 (2004). Eurocode 2: Design of concrete structures – Part 1-1: General rules and rules for buildings. Brussels: European Committee for Standardisation.

[41] J. Pereiro-Barceló, J.L. Bonet, Ni-Ti SMA bars behaviour under compression, Constr. Build. Mater. 155 (2017) 348–362, https://doi.org/10.1016/j.conbuildmat.2017.08.083.